Constraints on the annihilation cross section of dark matter particles from anisotropies in the diffuse gamma-ray background measured with Fermi-LAT

Ando, S.; Komatsu, E.

DOI
10.1103/PhysRevD.87.123539

Publication date
2013

Document Version
Final published version

Published in
Physical Review D. Particles, Fields, Gravitation, and Cosmology

PHYSICAL REVIEW D **87,** 123539 (2013)

Constraints on the annihilation cross section of dark matter particles from anisotropies in the diffuse gamma-ray background measured with Fermi-LAT

Shin'ichiro Ando

Gravitation Astroparticle Physics Amsterdam (GRAPPA) and Institute for Theoretical Physics, University of Amsterdam, 1090 GL Amsterdam, Netherlands

Eiichiro Komatsu

Max-Planck-Institut für Astrophysik, Karl-Schwarzschild Straße 1, 85741 Garching, Germany; Kavli Institute for the Physics and Mathematics of the Universe (Kavli IPMU, WPI), Todai Institutes for Advanced Study, The University of Tokyo, Kashiwa 277-8583, Japan; and Texas Cosmology Center and the Department of Astronomy, The University of Texas at Austin, 1 University Station, C1400, Austin, Texas 78712, USA

(Received 7 February 2013; published 28 June 2013)

Annihilation of dark matter particles in cosmological halos (including the halo of the Milky Way) contributes to the diffuse gamma-ray background (DGRB). As this contribution will appear anisotropic in the sky, one can use the angular power spectrum of anisotropies in the DGRB to constrain the properties of dark matter particles. By comparing the updated analytic model of the angular power spectrum of the DGRB from dark matter annihilation with the power spectrum recently measured from the 22-month data of the Fermi Large Area Telescope (LAT), we place upper limits on the annihilation cross section of dark matter particles as a function of dark matter masses. We find that the current data exclude $\langle\sigma v\rangle \gtrsim 10^{-25}$ cm^3 s^{-1} for annihilation into $b\bar{b}$ at the dark matter mass of 10 GeV, which is a factor of 3 times larger than the canonical cross section. The limits are weaker for larger dark matter masses. The limits can be improved further with more Fermi-LAT data as well as by using the power spectrum at lower multipoles ($\ell \lesssim 150$), which are currently not used due to a potential Galactic foreground contamination.

DOI: 10.1103/PhysRevD.87.123539 PACS numbers: 95.35.+d, 95.85.Pw, 98.70.Vc

I. INTRODUCTION

Understanding the identity and nature of dark matter, which makes up more than 80% of the total matter density in the Universe, is a major goal of modern physics and cosmology. The most promising candidate for dark matter is weakly interacting massive particles (WIMPs), with which one can naturally explain the observed dark matter density using a simple thermal freeze-out argument [1]. If dark matter particles annihilate into standard model particles, as expected for most WIMP scenarios, one can indirectly detect and constrain properties of dark matter particles [1–3]. In this paper, we shall focus on high-energy (1–50 GeV) gamma-ray photons produced by the cascade of annihilation products.

Dark matter annihilation occurs in all cosmological halos, including the halo of the Milky Way, and thus contributes to the diffuse gamma-ray background (DGRB) [4–8]. Due to the large-scale structure of the Universe, the observed gamma-ray emission appears anisotropic in the sky in a predictable manner, which makes it easy to identify the dark matter origin of high-energy gamma rays in the sky [9] (also see Refs. [10–26]).

Recently, the Fermi-LAT Collaboration has measured the power spectrum of DGRB anisotropy from 22 months of data [27]. They have detected significant excesses of the angular power spectrum over the shot noise of photons for a multipole range between $\ell = 155$ and 504 and for multiple energy bins. A further study shows that most of these excesses come from unresolved blazars [28]. Subtracting the estimate of the blazar contribution, we have upper bounds on the residual anisotropy of the DGRB.

In this paper, we use the upper bounds on the power spectrum to constrain the annihilation cross section of dark matter particles. For this purpose, we update our theoretical framework for computing the angular power spectrum presented in Refs. [9,10,20] as follows:

(1) We use the results from recent numerical simulations (e.g., Ref. [29]) to model the mass function and spatial distribution of subhalos within a given host halo.
(2) We include contributions from both the extragalactic dark matter halos and the Galactic dark matter subhalos.
(3) We also include the cross correlation between dark matter annihilation signals and blazars. Although this term was often ignored in the literature (except for Ref. [10]), one should include this term for self-consistency: the same halo hosting a blazar also contains annihilating dark matter particles, and there is a spatial correlation between halos hosting blazars and those not hosting blazars but containing annihilating dark matter particles.

This paper is organized as follows. In Sec. II, we present the predicted angular power spectrum of the DGRB from

extragalactic dark matter halos and compare this to the data to find constraints on the annihilation cross section. In Sec. III, we discuss the contribution from the cross-correlation term with blazars. In Sec. IV, we present the predicted angular power spectrum of the DGRB from Galactic subhalos and find combined constraints on the annihilation cross section using extragalactic and Galactic contributions. We conclude in Sec. V. Throughout the paper, we adopt a flat cold dark matter model with a cosmological constant (ΛCDM) with the following cosmological parameters: $\Omega_m = 0.277$, $\Omega_\Lambda = 0.723$, $H_0 = 100h$ km s^{-1} Mpc^{-1}, $h = 0.7$, $n_s = 0.96$, and $\sigma_8 = 0.81$.

II. EXTRAGALACTIC CONTRIBUTION

In this section, we discuss the mean intensity and anisotropy of the DGRB from dark matter annihilation in extragalactic halos. Much of the calculations are based on our earlier work [9,10], but with extensions of the framework and significant updates on input models as explained below.

A. Mean intensity

The mean intensity of gamma rays from dark matter annihilation is given by

$$I(E) = \int d\chi W([1+z]E, \chi)\langle\delta^2\rangle, \tag{1}$$

which we define as the number of photons received per unit area, unit time, unit energy range, and unit solid angle, i.e., $I(E) = dN/(dAdtdEd\Omega)$. E is the energy of the photons; χ is the comoving distance to a source at redshift z [χ and z are used interchangeably through the relation $d\chi/dz = c/H(z)$]; and $\langle\delta^2\rangle$ is the variance of the overdensity field, $\delta = (\rho - \langle\rho\rangle)/\langle\rho\rangle$, and is often also referred to as an "intensity multiplier." $W(E, z)$ is the window function that contains particle physics information such as a velocity-averaged annihilation cross section times relative velocity, $\langle\sigma v\rangle$, a dark matter mass, $m_{\rm dm}$, and a gamma-ray spectrum per annihilation, $dN_{\gamma,\rm ann}/dE$:

$$W(E, z) = \frac{\langle\sigma v\rangle}{8\pi}\left(\frac{\Omega_{\rm dm}\rho_c}{m_{\rm dm}}\right)^2(1+z)^3\frac{dN_{\gamma,\rm ann}}{dE}e^{-\tau(E,z)}, \tag{2}$$

where $\Omega_{\rm dm} = 0.23$ is the density parameter of dark matter, and ρ_c is the critical density of the present Universe. Here, $\tau(E, z)$ is the optical depth for a gamma ray emitted at energy E, for which we adopt the model of Ref. [30]. Note that the annihilation cross section required to produce dark matter at the right relic density by the thermal freeze-out mechanism with S-wave annihilation is $\langle\sigma v\rangle \simeq 3\times10^{-26}$ cm^3 s^{-1}, which is largely independent of the dark matter mass [1].[1]

[1]More recent study shows that the canonical cross section is 2.2×10^{-26} cm^3 s^{-1} [31].

The intensity multiplier is

$$\langle\delta^2\rangle = \left(\frac{1}{\Omega_m\rho_c}\right)^2\int dM\frac{dn(M,z)}{dM}[1+b_{\rm sh}(M)] \times\int dV\rho^2_{\rm host}(r|M), \tag{3}$$

where M is the virial mass, dn/dM is the halo mass function, for which we adopt an ellipsoidal collapse model [32,33], $\rho_{\rm host}(r|M)$ is the density profile of a host halo of mass M, r is the comoving radius from the halo center, and $b_{\rm sh}(M)$ is a boost factor due to annihilation in subhalos.

We adopt a Navarro-Frenk-White (NFW) [34] profile for host halos,

$$\rho_{\rm host}(r) = \frac{\rho_s}{(r/r_s)(r/r_s+1)^2}, \tag{4}$$

where ρ_s and r_s are the scale density and the scale radius, respectively, and this relation holds out to the virial radius, $r_{\rm vir}$, which, in turn, is given as a function of M and z through the relation $M = 4\pi r^3_{\rm vir}\Delta_{\rm vir}(z)\rho_c(z)/3$, with $\Delta_{\rm vir}(z) = 18\pi^2 + 82d - 39d^2$ and $d = \Omega_m(1+z)^3/[\Omega_m(1+z)^3 + \Omega_\Lambda] - 1$ [35].

The scale radius is defined as $r_s = r_{\rm vir}/c_{\rm vir}$, where $c_{\rm vir}(M, z)$ is the concentration parameter, for which we adopt the model of Ref. [36] for masses below $2.5\times10^{14}M_\odot$ and that of Ref. [37] otherwise. By taking the volume integral of the density profile, $\rho_{\rm host}(r)$, out to $r_{\rm vir}$ and equating it to M, we obtain the scale density as

$$\rho_s = \frac{M}{4\pi r_s^3}\left[\ln(1+c_{\rm vir}) - \frac{c_{\rm vir}}{1+c_{\rm vir}}\right]^{-1}. \tag{5}$$

The volume integral of the density squared has an analytic form:

$$\int dV\rho^2_{\rm host} = \frac{4\pi r_s^3\rho_s^2}{3}\left[1 - \frac{1}{(1+c_{\rm vir})^3}\right]. \tag{6}$$

The gamma-ray intensity is further boosted by annihilation in subhalos, which is represented by the boost factor, $b_{\rm sh}(M)$, for which we adopt a fitting formula based on results of recent numerical simulations [29]: $b_{\rm sh} \approx 110(M_{200}/10^{12}M_\odot)^{0.39}$, where M_{200} is an enclosed mass within a radius r_{200} in which the average density is 200 times the critical density; there is a simple relation between M_{200} and the virial mass M [38]. This boost is realized if the subhalo mass function extends down to Earth-mass scales, $M_{\rm sh,min} = 10^{-6}M_\odot$, which is a typical cutoff scale for the neutralino dark matter [39–42], and we adopt this value throughout the paper unless otherwise stated. We note, however, that the boost factor strongly depends on the minimum subhalo mass chosen, $b_{\rm sh} \propto M^{-0.2}_{\rm sh,min}$ [29]. Given that a wide range of minimum subhalo mass is still allowed, as small as $\sim10^{-12}M_\odot$ [43], the annihilation rate may be boosted even further.

Figure 1 shows the integrand of Eq. (3) as a function of the virial mass, M, for various redshifts, z. Namely, this

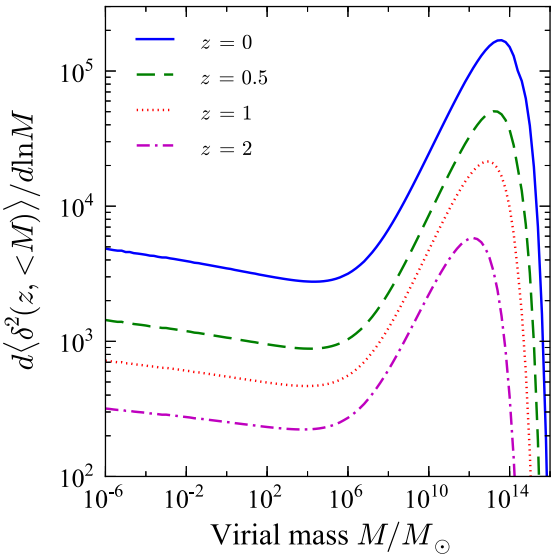

FIG. 1 (color online). Contribution to the intensity multiplier, $\langle\delta^2\rangle$ [Eq. (3)], from different mass ranges at various redshifts.

shows what fraction of $\langle\delta^2\rangle$ is contributed from which mass ranges. As can be seen from this figure, the dominant contribution comes from cluster-sized halos ($M \sim 10^{14} M_\odot$) at $z \sim 0$ and galaxy-sized halos ($M \sim 10^{12} M_\odot$) at $z \sim 2$. This is mainly because of the boost due to annihilation in subhalos. In Fig. 2, we compare the contribution from the host halos (dashed line) and that from the host halos and subhalos (solid line) at $z = 0$. If there are no gamma rays from subhalos, then the mean intensity would be dominated by the smallest dark matter halos.

Figure 3 shows the intensity multiplier $\langle\delta^2\rangle$ as a function of redshifts for the cases with and without subhalo

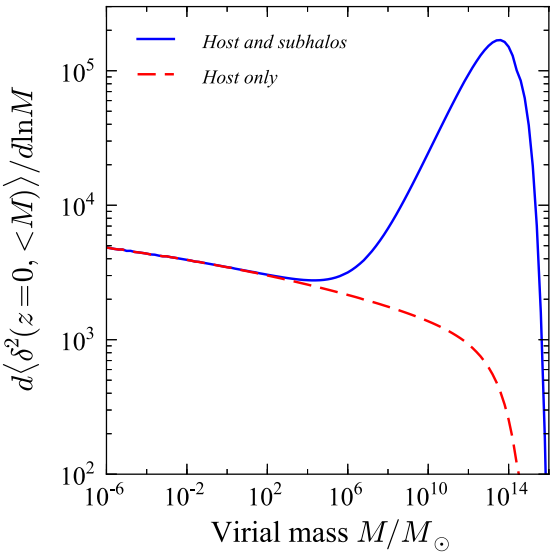

FIG. 2 (color online). Contributions to the intensity multiplier, $\langle\delta^2\rangle$ [Eq. (3)], from host halos (dashed line) and host halos and subhalos (solid line) at $z = 0$. The solid line is the same as that in Fig. 1.

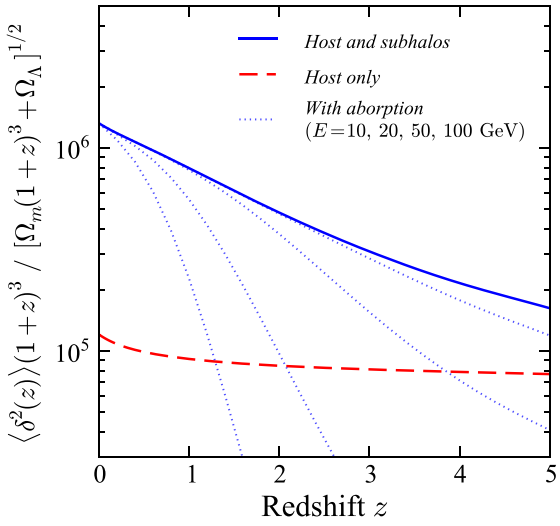

FIG. 3 (color online). Intensity multiplier as a function of redshifts. The solid line shows the total intensity multiplier from host halos and subhalos, while the dashed line shows the intensity multiplier only from host halos. The dotted lines show the total intensity multiplier multiplied by the absorption factors at various energies ($E = 100$, 50, 20, and 10 GeV from left to right).

contributions. Here we multiply $\langle\delta^2\rangle$ by $(1+z)^3/\sqrt{\Omega_m(1+z)^3+\Omega_\Lambda}$ to show contributions to the mean intensity from different redshift ranges. One can see that the presence of subhalos boosts the intensity by a factor of 10 at low redshifts, and by a factor of $\sim$2 even at $z = 5$. Since cluster-sized halos host most subhalos and they form later, the contribution from the low-redshift regime increases relatively more compared with the host-only case. The dotted lines are further multiplied by the absorption factor, $e^{-\tau}$, for observed energies of $E = 10$, 20, 50, and 100 GeV. There is little absorption for photons received below 10 GeV, but this effect is significant for energies above tens of GeV and should be taken into account.

Figure 4 shows the predicted mean intensity of the DGRB from dark matter annihilation with $m_{\rm dm} = 100$ GeV, $\langle\sigma v\rangle = 3 \times 10^{-26}$ cm^3 s^{-1}, and the $b\bar{b}$ annihilation channel. This model gives the dark matter contribution that is as large as 10% of the mean intensity measured by Fermi-LAT [44] at $E \sim 10$ GeV. This contribution is quite significant, given that even the most dominant contributors known to date, i.e., unresolved blazars, contribute to the DGRB at around the same level [45].

B. Angular power spectrum

The angular power spectrum at a given multipole, ℓ, is given by

$$C_\ell(E) = \int \frac{d\chi}{\chi^2} W^2([1+z]E, z) P_{\delta^2}\left(k = \frac{\ell}{\chi}, z\right). \quad (7)$$

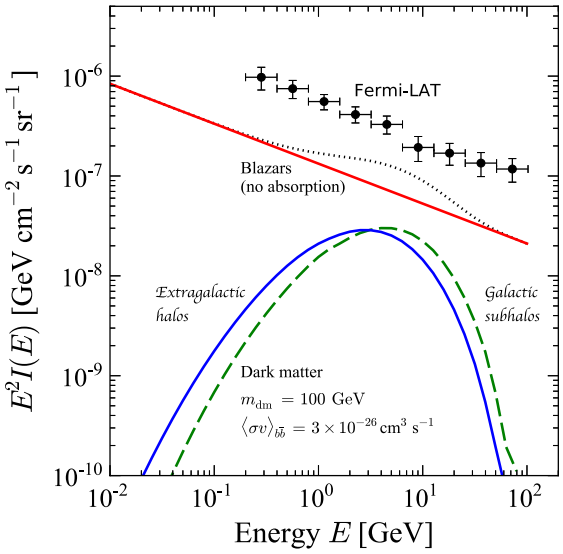

FIG. 4 (color online). Predicted mean intensity of the DGRB from dark matter annihilation via the $b\bar{b}$ channel. The dark matter mass is $m_{\rm dm} = 100$ GeV, and the cross section is at its canonical value, $\langle\sigma v\rangle = 3\times10^{-26}$ cm^3 s^{-1}. The solid line shows the extragalactic contribution (from both host halos and subhalos), while the dashed line shows the Galactic subhalo contribution (no smooth Galactic contribution is included). The Fermi-LAT data [44] as well as the contribution from unresolved blazars are also shown for comparison.

Following conventions of recent publications (e.g., Ref. [27]), our definition of the angular power spectrum [Eq. (7)] has the units of $(\text{cm}^{-2}\,\text{s}^{-1}\,\text{sr}^{-1}\,\text{GeV}^{-1})^2$ sr, which is referred to as the *intensity* angular power spectrum.[2] In order to obtain the *fluctuation* angular power spectrum that has units of sr and is adopted in the earlier papers (e.g., Ref. [9]), one simply divides the intensity power spectrum by the mean intensity squared, $I^2(E)$.

Here, $P_{\delta^2}(k, z)$ is the power spectrum of the overdensity squared, δ^2, which can be divided into one- and two-halo terms [9]:

$$P_{\delta^2}(k, z) = P^{1\,\rm h}_{\delta^2}(k, z) + P^{2\,\rm h}_{\delta^2}(k, z). \tag{8}$$

The one-halo term correlates two points in one identical halo, whereas the two-halo term does the same in two distinct halos. Correspondingly, the angular power spectrum is also divided into two terms:

$$C_\ell(E) = C^{1\,\rm h}_\ell(E) + C^{2\,\rm h}_\ell(E). \tag{9}$$

These two terms of the power spectrum can be explicitly written as

$$P^{1\,\rm h}_{\delta^2}(k, z) = \left(\frac{1}{\Omega_m\rho_c}\right)^4 \int dM \frac{dn(M, z)}{dM} |\tilde{u}(k|M)|^2 \times \left[(1 + b_{\rm sh}(M)) \int dV \rho^2_{\rm host}(r|M)\right]^2, \tag{10}$$

$$P^{2\,\rm h}_{\delta^2}(k, z) = \left[\left(\frac{1}{\Omega_m\rho_c}\right)^2 \int dM \frac{dn(M, z)}{dM} \tilde{u}(k|M) b_1(M, z) \times (1 + b_{\rm sh}(M)) \int dV \rho^2_{\rm host}(r|M)\right]^2 P_{\rm lin}(k, z), \tag{11}$$

where $P_{\rm lin}(k, z)$ is the linear power spectrum of the matter density field δ, and $b_1(M, z)$ is the linear halo bias [33]. The power spectrum of δ^2, P_{δ^2}, depends on profiles of density *squared* in a halo of mass M, $u(r|M)$, where $u(r|M)$ is normalized such that its volume integration becomes unity; $\tilde{u}(k|M)$ is the Fourier transform of $u(r|M)$.

Fourier transform of the density-squared profile, $\tilde{u}(k|M)$, is the sum of the density-squared profiles of the host halo and subhalos weighted by a fractional luminosity of each component:

$$\tilde{u}(k|M) = \frac{\tilde{u}_{\rm host}(k|M) + b_{\rm sh}(M)\tilde{u}_{\rm sh}(k|M)}{1 + b_{\rm sh}(M)}. \tag{12}$$

Here, we ignore a contribution from the cross term, $2\rho_{\rm host}(r)\rho_{\rm sh}(r)$, which is important only when $\rho_{\rm host}(r) \sim \rho_{\rm sh}(r)$ at the same radius, r. Given that spatial distributions of the host halo and subhalo contributions are quite different (the host halo being important inside the scale radius and the subhalos being important outside), this approximation is very good. (See the Appendix for the contribution of the cross term.)

Fourier transform of the host halo profile, $u_{\rm host}(r) \propto \rho^2_{\rm host}(r)$, has an analytic form [9], but here we use an even simpler fitting formula,

$$\tilde{u}_{\rm host}(k|M) = \frac{1}{[1 + a(kr_s)^{2/b}]^b}, \tag{13}$$

with $a = 0.13$ and $b = 0.7$, which is largely independent of $c_{\rm vir}$ [20]. On the other hand, we obtain the density-squared profile of subhalos, $u_{\rm sh}(r|M)$, by deprojecting the surface brightness profiles of numerical simulations [29,46], assuming spherical symmetry as follows:

$$u_{\rm sh}(r) \propto \begin{cases} \left[\left(\frac{r}{r_{200}}\right)^2 + \frac{1}{16}\right]^{-3/2}, & \text{for } r \le r_{200}, \\ \left(\frac{16}{17}\right)^{3/2}\left(\frac{r}{r_{200}}\right)^{-1} e^{-\eta(r/r_{200}-1)}, & \text{for } r > r_{200}, \end{cases} \tag{14}$$

with $\eta = 2.78$. Note that the distribution of subhalos is typically more extended than the density profile of the host halo. Its Fourier transform is

[2]When we compare theoretical predictions with the data, we must integrate a gamma-ray intensity in a given direction over energy within a given energy bin. We do this by replacing the window function, $W([1 + z]E, z)$, in Eqs. (1) and (7) with the window function integrated over a given energy range. This gives C_ℓ in units of $(\text{cm}^{-2}\,\text{s}^{-1}\,\text{sr}^{-1})^2$ sr.

$$\tilde{u}_{\rm sh}(k|M) = A\left[\int_0^1 dx \frac{x^2}{(x^2+1/16)^{3/2}} \frac{\sin(\kappa x)}{\kappa x} + \frac{64}{17^{3/2}} \frac{\kappa\cos\kappa + \eta\sin\kappa}{\kappa(\kappa^2+\eta^2)}\right], \quad (15)$$

where $\kappa \equiv k r_{200}$ and $A \approx 0.64$ is the normalization constant such that $\tilde{u}_{\rm sh}(0) = 1$.

Figure 5 shows $\tilde{u}(k|M)$ for various host-halo masses, M. When $\tilde{u}(k)$ is close to unity (for small k), the halo can be regarded as a point source. On the other hand, when $\tilde{u}(k)$ deviates significantly from unity at a given wave number k, the source extension cannot be ignored at that wave number, and the power spectrum (especially the one-halo term) is suppressed. Figure 5 shows that $\tilde{u}(k)$ is larger for smaller host halos, which are less extended. It also shows that the contributions from subhalos are more important for larger host halos. As the distribution of subhalos is more extended than the density profile of the host halo, the subhalo contribution dominates at small k and the host-halo dominates at large k. This makes a hump at scales corresponding to the scale radius, r_s. In other words, annihilation from the smooth host-halo component dominates inside the scale radius, where subhalos are tidally disrupted.

Figure 6 shows the integrand of the one-halo power spectrum of δ^2, $dP^{1\,\rm h}_{\delta^2}(k, <M)/d\ln M$ [Eq. (10)], at $z = 0$ for various wave numbers, k. (Note that the lines are normalized at $M = 1M_\odot$, and thus it shows relative contributions rather than absolute.) The bulk of the contributions come from large-mass halos, and halos smaller than a typical dwarf size ($M < 10^6 M_\odot$) do not make any sizable contributions to any relevant ranges of k. This is particularly true for scales larger than a typical cluster size (i.e., $k \lesssim 1$ Mpc^{-1}). For smaller scales, on the other hand, the relative importance of large-mass halos is smaller, as large-mass halos are more extended, and thus the power from them is suppressed (as also shown in Fig. 5).

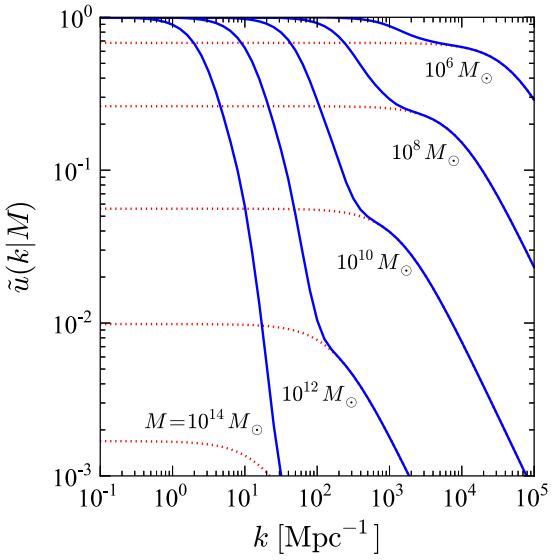

FIG. 5 (color online). Fourier transform of the density-squared profile, $\tilde{u}(k|M)$, for various host-halo masses. The solid lines show the total (host halo and subhalos) profile, whereas the dotted lines show the host-halo profiles. Note that the total $\tilde{u}(k|M)$ is normalized to unity at $k \to 0$, and thus the dotted lines do not approach unity at $k \to 0$ but approach $1/(1 + b_{\rm sh})$ [see Eq. (12)].

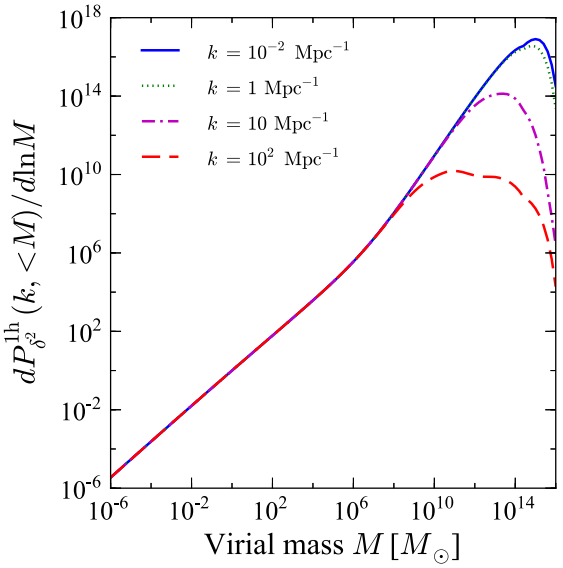

FIG. 6 (color online). Relative contributions to the one-halo power spectrum $P^{1\,\rm h}_{\delta^2}$ at $z = 0$ as a function of masses and wave numbers. The lines are normalized at $M = 1M_\odot$.

Figure 7 is the same as Fig. 6 for $k = 1$ Mpc^{-1}, but the host-halo contribution is also shown. We find that the impact of subhalos on the power spectrum is much greater than that on the mean intensity (as shown in Fig. 2), and it

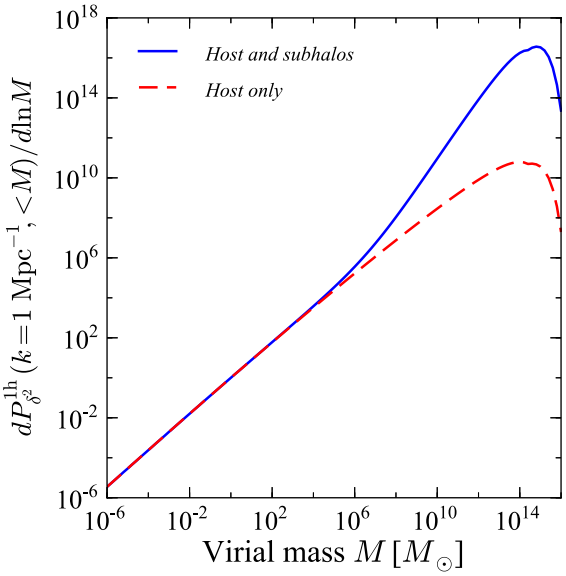

FIG. 7 (color online). The same as Fig. 6 for $k = 1$ Mpc^{-1}, but in comparison with the host-halo contribution.

can boost the power spectrum by almost 4 orders of magnitude at this particular wave number.

After being projected on the sky, the three-dimensional wave number, k, and the angular multipole, ℓ, are related by $k = \ell/\chi(z)$ for a given redshift, z [see Eq. (7)]. Note, however, that this simple relation is valid only for small angular scales, $\ell \gg 1$ (e.g., Refs. [9,10]), on which we mainly focus in this paper.

Figures 8 and 9 show the contributions to the angular power spectra at $\ell = 10$, 100, and 1000 from one-halo and two-halo terms, respectively, as a function of redshifts. To calculate a contribution to C_ℓ from a given z, we multiply P_{δ^2} by some combination of functions of redshift [see the integrand of Eq. (7) and also the redshift dependence in Eq. (2)]. We find that lower multipoles are dominated by nearby sources: one-halo terms at $\ell = 10$, 100, and 1000 are dominated by sources at $z \sim 0.002$, 0.02, and 0.2, respectively, whereas the dominant contributions to the two-halo term come from somewhat higher redshifts.

One should not, however, include contributions from arbitrarily small redshifts in the integral of Eq. (7), as cosmic variance in such small redshifts is so large that taking the ensemble average (as we do here) no longer makes sense. In addition, when a source is sufficiently close, it should give enough gamma-ray fluxes to be identified as an individual source which we can remove from the map. In the following discussion, we use three different minimum redshifts in the integration of Eq. (7): $z_{\rm min} = 0.001$, 0.003, and 0.01. The rms overdensity within radii corresponding to these three redshifts are 1.4, 0.74, and 0.28, respectively. Since none of these are much larger than 1, we can argue that our results by setting these lower cutoffs are not subject to strong cosmic variance. We also

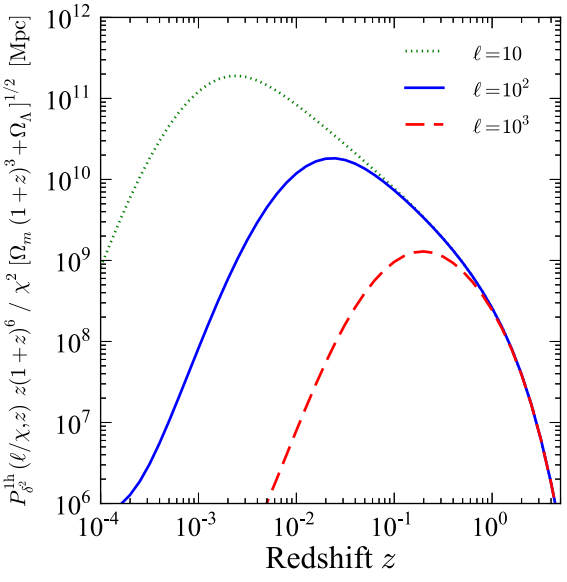

FIG. 8 (color online). One-halo contributions to the angular power spectrum, $C_\ell^{\rm 1\,h}$, at $\ell = 10$, 100, and 1000 as a function of redshifts.

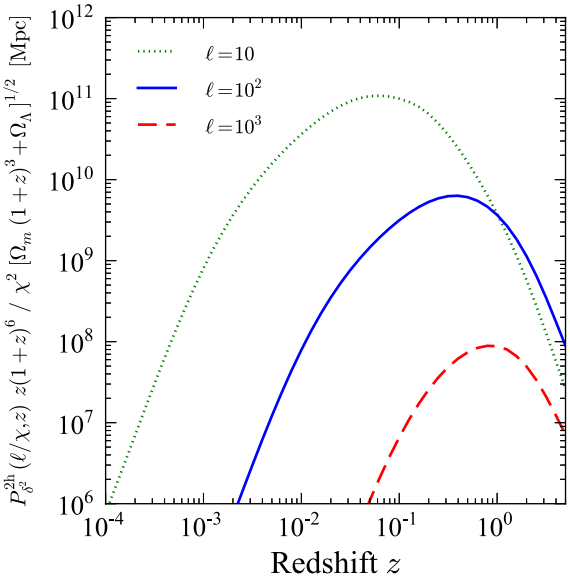

FIG. 9 (color online). The same as Fig. 8, but for the two-halo contributions to the angular power spectrum, $C_\ell^{\rm 2\,h}$.

note that, as we show below, this choice does not make any significant difference for the multipoles we consider ($\ell > 150$) in this paper.

In Fig. 10, we show both the one-halo and two-halo terms of the angular power spectrum, C_ℓ, integrated over the 5–10 GeV energy range, for three different values of $z_{\rm min} = 0.001$, 0.003, and 0.01. The particle physics parameters are $\langle\sigma v\rangle = 3 \times 10^{-26}$ cm^3 s^{-1} and $m_{\rm dm} = 100$ GeV, and we assume the $b\bar{b}$ annihilation channel. Note that C_ℓ scales as $\langle\sigma v\rangle^2$. Taking smaller $z_{\rm min}$ increases the power at large angular scales, in particular for the one-halo term, because of the contributions from closer, more extended halos. For the rest of this paper, we shall use $z_{\rm min} = 0.003$ for definiteness.

The thick solid line in Fig. 10 shows the upper limits on the angular power spectrum [27] (with the blazar contribution subtracted [28]) between $\ell = 155$ and 504 for 5–10.4 GeV, $C_{155\le\ell\le504} \le 8 \times 10^{-20}$(cm^{-2} s^{-1} sr^{-1})^2 sr. The current upper limits in 5–10.4 GeV, whose energy region is most sensitive to dark matter particles with $m_{\rm dm} = 100$ GeV annihilating into $b\bar{b}$ (see Fig. 4), are 3 orders of magnitude larger than the prediction with the canonical particle physics parameters. Recalling $C_\ell \propto \langle\sigma v\rangle^2$, we find an upper limit on the cross section of $\langle\sigma v\rangle \lesssim 8 \times 10^{-25}$ cm^3 s^{-1} for the 100-GeV dark matter annihilating into $b\bar{b}$.

The blazar-subtracted upper limits on the angular power spectrum are available in several energy bands, 1.04–1.99 GeV, 1.99–5 GeV, 5–10.4 GeV, and 10.4–50 GeV [28]. In Fig. 11, we show the combined upper limits on the annihilation cross section for the $b\bar{b}$ channel, $\langle\sigma v\rangle_{b\bar{b}}$, as a function of the dark matter masses, $m_{\rm dm}$, using all the available data on the power spectrum. (Note that the model is still based only on the extragalactic contribution.)

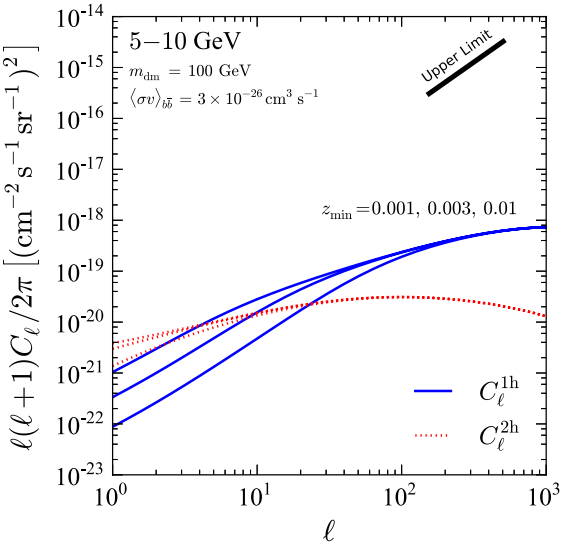

FIG. 10 (color online). Predicted angular power spectrum of the DGRB from dark matter annihilation in extragalactic halos from the entire sky, integrated over the energy range between 5 GeV and 10 GeV. (This energy range is most sensitive to dark matter particles with $m_{\rm dm} = 100$ GeV annihilating into $b\bar{b}$; see Fig. 4.) The one-halo (solid) and two-halo (dotted) terms are shown separately, for three different minimum redshifts $z_{\rm min} = 0.003$, 0.001, and 0.01 (from top to bottom lines). The particle physics parameters are $\langle\sigma v\rangle = 3\times10^{-26}$ cm^3 s^{-1} and $m_{\rm dm} = 100$ GeV, and the $b\bar{b}$ annihilation channel is assumed. For comparison, the thick solid line shows the upper limit on the angular power spectrum in $155 \le \ell \le 504$ from the 22-month data of Fermi-LAT [27] with the blazar contribution subtracted [28].

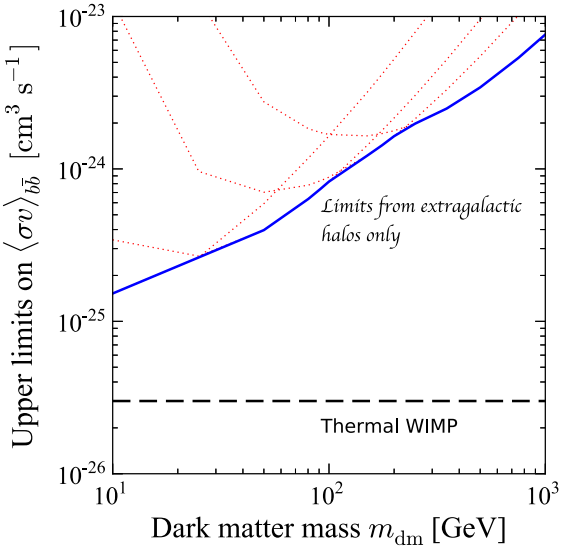

FIG. 11 (color online). Upper limits on the annihilation cross section into the $b\bar{b}$ final state as a function of the dark matter masses, $m_{\rm dm}$. The limits are obtained from the measurement of the angular power spectrum at $\ell = 155$ [27] with the blazar contribution subtracted [28], and the theoretical model of dark matter annihilation from extragalactic halos. The dotted lines show the limits from different energy ranges: 1.04–1.99 GeV, 1.99–5 GeV, 5–10.4 GeV, and 10.4–50 GeV from bottom to top at the low-mass region. The solid line shows the combined limits, and the horizontal dashed line shows the canonical cross section for the thermal freeze-out scenario.

We calculate the upper limit on the cross section such that the predicted C_ℓ at $\ell = 155$ (the lowest multipole at which the measurement is reported) is equal to the 2σ upper limit reported by Ref. [28]. The limits from each energy range are shown separately as the dotted lines. The combined limits shown as the solid line are simply the best of the four limits at a given dark matter mass. A more optimal analysis would improve these limits.

These results depend on assumed subhalo models. In particular, a different number of subhalos will change them significantly. Therefore, we also investigated with another value of the assumed minimum subhalo mass, $M_{\rm sh,min} = 10^{-10}M_\odot$, which is well within the currently preferred WIMP framework [43]. In this case, the rate of annihilation and the mean intensity are boosted by a factor of $\sim$6. Numerical simulations suggest that the radial profile of the subhalo distribution may not change (e.g., Ref. [29]), and hence we use the same formula as Eq. (14). The upper limits on the annihilation cross section with the angular power spectrum are then improved by a factor of $\sim$6.3, almost independently of the dark matter mass. The canonical cross section for thermal WIMPs is now excluded for the low-mass regime. As yet another extreme scenario, we also repeated the calculations for the no-subhalo case, where we have contributions from smooth host halos only. Compared with our canonical subhalo model (i.e., $M_{\rm sh,min} = 10^{-6}M_\odot$), we find that the mean intensity gets reduced by an order of magnitude. The limits of the annihilation cross section from analysis of the angular power spectrum become less stringent by a factor of $\sim$72 (60) for $m_{\rm dm} = 10$ GeV (1 TeV).

III. CROSS CORRELATION BETWEEN DARK MATTER AND BLAZARS

As astrophysical gamma-ray sources, such as blazars associated with supermassive black holes at the centers of galaxies, reside in dark matter halos, there is a spatial correlation between gamma rays from dark matter annihilation and blazars. The angular power spectrum of dark matter annihilation including the cross correlation, which is equal to the total power spectrum minus the blazar power spectrum, is given by

$$C_\ell^{\rm dm} \equiv C_\ell - C_\ell^{\rm blazar} = C_\ell^{\rm 1\,h} + C_\ell^{\rm 2\,h} + 2C_\ell^{\times}, \qquad (16)$$

where $C_\ell^{\times}$ is the cross power spectrum computed from[3]

[3]We include blazars in the cross correlation, ignoring other sources of gamma rays. This may be justified, as blazars are so far known to be the most dominant extragalactic gamma-ray sources in the GeV energy regime. Other promising sources include star-forming galaxies [21,47–50].

$$C_\ell^\times(E) = \int \frac{d\chi}{\chi^2} W_B([1+z]E, z) W_{\rm dm}([1+z]E, z) \times P_\times\left(k = \frac{\ell}{\chi}, z\right), \quad (17)$$

where the subscripts "B" and "dm" denote blazars and dark matter, respectively. Here, $W_{\rm dm}$ is the same as Eq. (2), while W_B is the window function for the mean intensity of blazars [similarly defined as Eq. (1) but replacing $\langle\delta^2\rangle$ with 1]:

$$W_B([1+z]E, z) = \chi^2 \int_0^{\mathcal{L}(\mathcal{F}_{E,\rm lim}, z)} d\mathcal{L}\Phi_E(\mathcal{L}, z)\mathcal{F}_E(\mathcal{L}, z), \quad (18)$$

where $\mathcal{L}$ is the differential luminosity (i.e., luminosity per unit energy) at a given energy E, $\mathcal{F}_E$ is the differential flux, and $\Phi_E(\mathcal{L}, z)$ is the gamma-ray luminosity function of blazars. The upper limit of the integral, $\mathcal{L}(\mathcal{F}_E, z)$, is the luminosity giving the flux corresponding to the point-source sensitivity of Fermi-LAT at a given redshift z, for which we adopt 10^{-8} cm^{-2} s^{-1} above 100 MeV. More formal definitions of these quantities can be found in Ref. [10].

The three-dimensional cross power spectrum is

$$\begin{aligned} P_\times(k, z) &= \langle b_B(z)\rangle\left[\left(\frac{1}{\Omega_m\rho_c}\right)^2 \int dM \frac{dn}{dM}(M, z)\tilde{u}(k|M) \times b_1(M, z)(1 + b_{\rm sh}(M)) \times \int dV \rho^2_{\rm host}(r|M)\right] P_{\rm lin}(k, z) \\ &= \langle b_B(z)\rangle\sqrt{P^{2\,\rm h}_{\delta^2}(k, z)P_{\rm lin}(k, z)}, \end{aligned} \quad (19)$$

where $\langle b_B(z)\rangle$ is the blazar bias averaged over the luminosity function and the flux as follows:

$$\langle b_B(z)\rangle = \frac{\int d\mathcal{L}\Phi_E(\mathcal{L}, z)\mathcal{F}_E(\mathcal{L}, z)b_B(\mathcal{L}, z)}{\int d\mathcal{L}\Phi_E(\mathcal{L}, z)\mathcal{F}_E(\mathcal{L}, z)}, \quad (20)$$

with the luminosity-dependent bias, $b_B(\mathcal{L}, z)$, and the same upper and lower limits of integration as those in Eq. (18).

Note that this power spectrum [Eq. (19)] includes the two-halo term only. While the one-halo term, where dark matter annihilation happens in the same halo that hosts a blazar, also exists, the previous study [10] shows that the one-halo term of the cross correlation is much smaller than the two-halo term; thus, we shall ignore the one-halo term of the cross power spectrum.

For the luminosity function, $\Phi_E(\mathcal{L}, z)$, we adopt the luminosity-dependent density-evolution model [11,51] with the gamma-ray spectra assumed to be a power law with an index of 2.4, which is in agreement with the spectrum of resolved blazars as well as that of the DGRB.[4] Compared with the earlier study [11], where the luminosity function was based on *pre*-Fermi data, we here adopt different values for parameters of the luminosity function ($\kappa = 10^{-4}$, $q = 3.5$, and $\gamma_1 = 1.05$) such that the model reproduces the flux distribution of blazars resolved by Fermi [45].

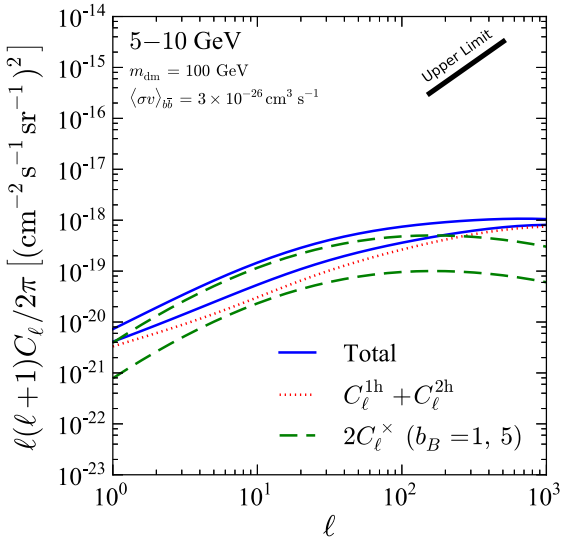

FIG. 12 (color online). Predicted angular power spectra of the DGRB in 5–10 GeV from dark matter annihilation only (dotted), dark matter–blazar cross correlation (dashed), and the sum of the two (solid). The particle physics parameters are the same as those in Fig. 10. For the blazar bias, we use $b_B = 1$ (bottom dashed/solid) and 5 (top dashed/solid).

In Fig. 4, we show the blazar contribution to the mean intensity. It is difficult to explain the DGRB intensity measured by Fermi with blazars alone, in agreement with the previous study [45,54].

Figure 12 shows the angular power spectra from the cross correlation with $\langle b_B\rangle = 1$ and 5, for the energy range between 5 GeV and 10 GeV. The particle physics parameters are the same as those in Fig. 10. We find that, if the annihilation cross section is around the canonical value required to produce dark matter particles at the right abundance by the thermal freeze-out mechanism, then the cross-correlation term cannot be ignored. This is particularly important when the bias of blazars is as high as 5.

As the dark matter term ($C_\ell^{1\,\rm h} + C_\ell^{2\,\rm h} \propto \langle\sigma v\rangle^2$) and the cross-correlation term ($C_\ell^\times \propto \langle\sigma v\rangle$) scale with $\langle\sigma v\rangle$ differently, one may ask, "At which value of the annihilation cross section does the cross-correlation term become important?" Figure 13 shows $C_{\ell=155}$ divided by the upper

[4]More elaborated spectra in combination with the luminosity function and the DGRB intensity are studied in Refs. [52,53].

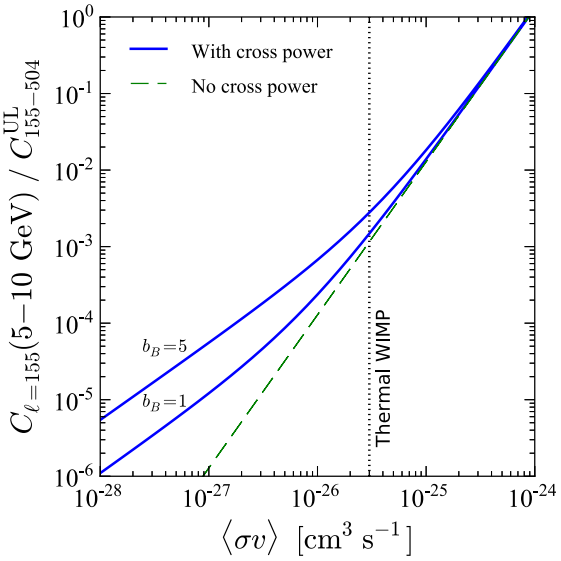

FIG. 13 (color online). Predicted angular power spectrum at $\ell = 155$ in 5–10 GeV divided by the current upper limit, $C^{\mathrm{UL}}_{155\le\ell\le504}$, as a function of the annihilation cross section, $\langle\sigma v\rangle$. The solid lines include the dark matter–blazar cross correlation with $\langle b_B\rangle = 1$ and 5, while the dashed line does not. The vertical dotted line shows the canonical cross section for thermal WIMPs.

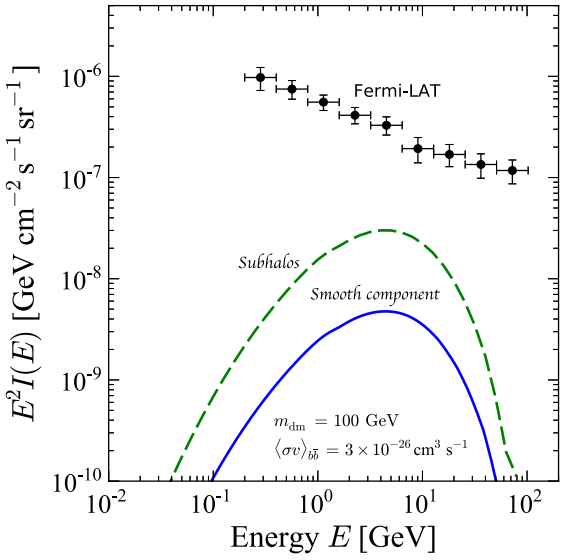

FIG. 14 (color online). The same as Fig. 4, but for the Galactic smooth component in the high Galactic latitude region outside of $|b| > 30$ deg (solid). The dashed line is the same as that in Fig. 4.

limit, $C^{\mathrm{UL}}_{155\le\ell\le504}$, for 5–10 GeV. The dashed line is without the cross correlation, while the solid lines are with the cross correlation with bias of 1 and 5. We find that the dark matter term dominates at $\langle\sigma v\rangle \gtrsim 3\times10^{-26}\ \mathrm{cm}^3\ \mathrm{s}^{-1}$, whereas the cross-correlation term dominates at lower cross sections.

IV. GALACTIC CONTRIBUTION

Annihilation signals from subhalos in the Galactic halo containing the Milky Way are typically comparable to, or even greater than, the extragalactic contribution [7,8,15,18,20]; thus, we must also take the Galactic subhalo contribution into account. We shall follow an analytic treatment presented in Ref. [20].

On the other hand, we do not include the contribution from a smooth density profile of the host halo of the Milky Way in our calculation. In the anisotropy analysis of the Fermi-LAT data [27], the low Galactic latitude region of $|b| \le 30$ deg is masked. Using a density profile of the smooth Galactic component of Ref. [20], we find that this mask brings the smooth contribution to the mean intensity down to about 10% of the subhalo contribution, as shown in Fig. 14. As the smooth component does not have much power on small angular scales, it can be safely ignored for $\ell \gtrsim 100$ (but it can be comparable to the subhalo and extragalactic contributions on large angular scales, $\ell \lesssim 10$).

The *angle-averaged* mean intensity from dark matter annihilation in Galactic subhalos can be computed from

$$I_{\mathrm{sh}} = \int dL \int_{s_*(L)}^{r_{\mathrm{vir,MW}}} ds \frac{d\overline{n_{\mathrm{sh}}}(L,s)}{dL} L, \tag{21}$$

where L is the gamma-ray luminosity of a subhalo, s is the line-of-sight coordinates, and $d\overline{n_{\mathrm{sh}}}/dL$ is the angle-averaged luminosity function of subhalos. The lower limit of the line-of-sight integral, $s_*(L)$, corresponds to the flux sensitivity of Fermi-LAT, i.e., $L = 4\pi s_*^2 F_{\mathrm{sens}}$.

The subhalo luminosity, L, is related to the subhalo mass, M, via

$$L = B_{\mathrm{sh}} \frac{\langle\sigma v\rangle N_{\gamma,\mathrm{ann}}}{2m_{\mathrm{dm}}^2} \int dV_{\mathrm{sh}} \rho_{\mathrm{sh}}^2(r_{\mathrm{sh}}|M), \tag{22}$$

where $r_{\mathrm{vir,MW}}$ is the virial radius of the Galactic halo, the subscripts "sh" denote subhalos, and B_{sh} is a boost factor due to the presence of substructure in subhalos (sub-subhalos).

We assume that the density profile of subhalos, ρ_{sh}, is well described by the NFW function [Eq. (4)]. Then, the volume integral of the density squared has the analytic form given by Eq. (6) with the concentration parameter, c_{vir}, replaced with c_{cut}, which corresponds to the cutoff radius of subhalos due to the tidal disruption, i.e., $c_{\mathrm{cut}} \equiv r_{\mathrm{cut}}/r_s$. With this mass-luminosity relation [Eq. (22)] and the subhalo mass function dn_{sh}/dM, one can compute the luminosity function. Most model inputs such as the

subhalo mass function, spatial distribution, and mass-concentration relation [$c_{\rm vir}(M)$] are adopted from recent numerical simulations of the Galactic halo, *Aquarius* [55]. More details on how to apply these models to gamma-ray computations are described in Ref. [20].

The intensity angular power spectrum is

$$C_\ell^{\rm sh} = \frac{1}{16\pi^2}\int dL \int \frac{ds}{s^2} L^2 \frac{d\overline{n_{\rm sh}}(L,s)}{dL} \left|\tilde{u}_{\rm sh}\left(\frac{\ell}{s}, M\right)\right|^2, \tag{23}$$

where $\tilde{u}_{\rm sh}(k, M)$ is the Fourier transform of the density-squared profile of the subhalo distribution, which is given by Eq. (13) if the density distribution of subhalos follows a NFW profile. Note that Eq. (23) only includes a "one-subhalo" term, where one correlates two points in one identical subhalo. There is, however, the two-subhalo term that correlates two points in two distinct subhalos, but this term is much smaller than the one-subhalo term at small angular scales [20].

Figure 15 shows the predicted angular power spectra from Galactic subhalos and extragalactic halos (but not including the cross correlation). We have used the canonical model of the Galactic subhalos given in Ref. [55], which has the mass resolution of about $4 \times 10^4 M_\odot$. We have extrapolated their result down to the Earth-mass scale (model A1 of Ref. [20]). The intensity power spectrum is about the same for both the extragalactic and Galactic components, with the latter slightly larger in the angular scales constrained by Fermi-LAT.

In Fig. 16, we show the limits on $\langle\sigma v\rangle$ from the Fermi-LAT data, taking into account both the extragalactic and

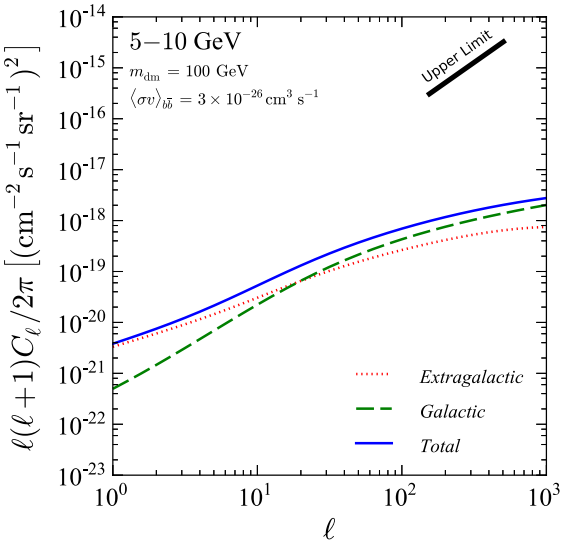

FIG. 15 (color online). Predicted angular power spectra of the DGRB in 5–10 GeV from dark matter annihilation in extragalactic halos (dotted), Galactic subhalos (dashed), and the sum of the two (solid).

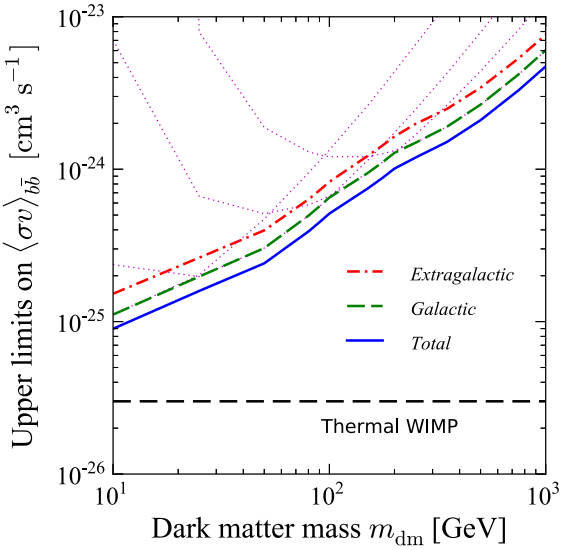

FIG. 16 (color online). The same as Fig. 11, but for the limits obtained from the Galactic subhalos (dashed), extragalactic halos (dot-dashed), and the sum of the two (solid). The dot-dashed line is the same as the solid line in Fig. 11. The dotted lines show the Galactic subhalo limits from each of four energy bins.

Galactic terms. As expected, the limits from either alone are similar, and the combined limits improve by a factor of 2. In particular, for low-mass dark matter particles, the combined limits are only a factor of 3 larger than the canonical cross section. The limits are weaker for larger masses.

While our limits are not yet as stringent as those obtained from analyses of dwarf galaxies [56,57] or galaxy clusters [46,58], where the canonical cross section is already excluded for low-mass (∼10 GeV) dark matter particles, they are not so far away (i.e., only a factor of 3 to 4 worse). Also, our limits are derived in a completely different way: they are based on the diffuse emission rather than on individual objects, and they are based on anisotropy rather than on the mean intensity. It is certainly encouraging that the first limits using the DGRB anisotropy are already not so far away from the best limits.

V. CONCLUSIONS

In this paper, we have used the angular power spectrum of DGRB recently detected in the 22-month data of Fermi-LAT [27] to place limits on the annihilation cross section of dark matter particles as a function of dark matter masses. As dark matter annihilation occurs in all cosmological halos and subhalos, our model includes all the contributing terms in the extragalactic halos, the Galactic subhalos, and the cross correlation between dark matter annihilation and blazars. The smooth Galactic component is predicted to be

subdominant in the high Galactic region ($|b| > 30$ deg) and is ignored.

We have revised our earlier model of the extragalactic contribution by including the results from recent numerical simulations of the subhalo distribution [29]. Combined with the model of the Galactic subhalos of Ref. [20], we find that the Galactic and extragalactic contributions are comparable to each other. The cross correlation with blazars is important for annihilation cross sections smaller than the canonical value ($\langle\sigma v\rangle \lesssim 3 \times 10^{-26}$ cm^3 s^{-1}).

By comparing our model with the upper limit on the nonblazar contribution to the angular power spectrum of the DGRB [28], we find upper limits on the annihilation cross section as a function of dark matter masses as shown in Fig. 16. The current limit from anisotropy excludes regions of $\langle\sigma v\rangle \gtrsim 10^{-25}$ cm^3 s^{-1} at the dark matter mass of 10 GeV, which is only a factor of 3 larger than the canonical value. The limits are weaker for larger dark matter masses. The first limits from DGRB anisotropy that we find in this paper are already competitive with the best limits in the literature.

Our limits will improve as Fermi collects more data. At the same time, an improvement in the analysis can significantly improve our limits. Currently, the angular power spectrum on large angular scales, $\ell < 155$, is not used because of a potential contamination by the Galactic foreground emission (such as pion decay). As the angular power spectrum of the DGRB from dark matter annihilation, C_ℓ (without multiplying by ℓ^2), rises towards low multipoles, including the low-multipole data will significantly improve the limits. This line of investigation (i.e., a better characterization and removal of the Galactic foreground) should be pursued.

ACKNOWLEDGMENTS

The work of S. A. was supported by the GRAPPA Institute at the University of Amsterdam and by NWO through a Vidi Grant.

APPENDIX: EFFECT OF HOST-SUBHALO CROSS TERM

The dark matter annihilation signal is proportional to the density squared. When both host halo and subhalo contributions are present, one has the host-density-squared term, $\rho^2_{\rm host}$, the subhalo-density-squared term, $\rho^2_{\rm sh}$, and the host-subhalo cross term, $2\rho_{\rm host}\rho_{\rm sh}$. In our analysis, we have ignored the cross term [see Eq. (12)], as spatial distributions of the host halo and subhalo contributions are quite different (the host halo being important inside the scale radius and the subhalos being important outside). In this appendix, we quantify the importance of the cross term.

Figure 17 shows the density-squared profiles of a host halo, subhalos, and the cross term. As expected, the cross term becomes comparable to the other terms only within a narrow window in radii. For the host halo mass of $M = 10^{14} M_\odot$ and the redshift of $z = 0$, the cross term becomes comparable to the other terms at $r \sim 20$ kpc, which is 1/10 of the scale radius, $r_s = 210$ kpc. Fig. 18 shows the Fourier transform.

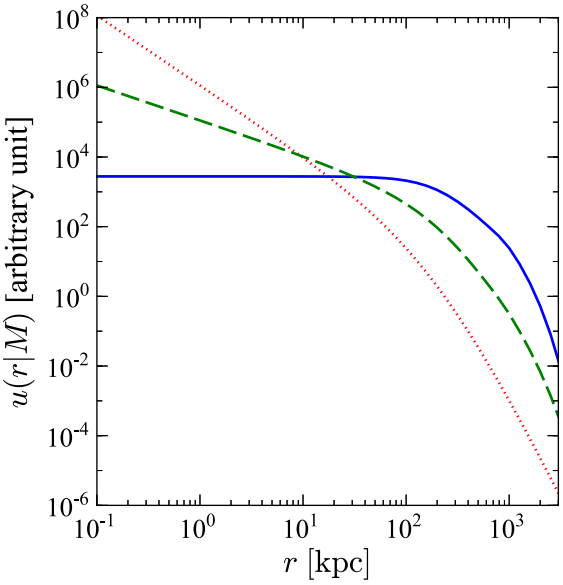

FIG. 17 (color online). Density-squared profiles of a host halo (dotted), subhalos (solid), and a host-subhalo cross term (dashed). The mass of the host halo is $M = 10^{14} M_\odot$, and the redshift is $z = 0$. The virial radius is 1.2 Mpc, and the scale radius is 210 kpc.

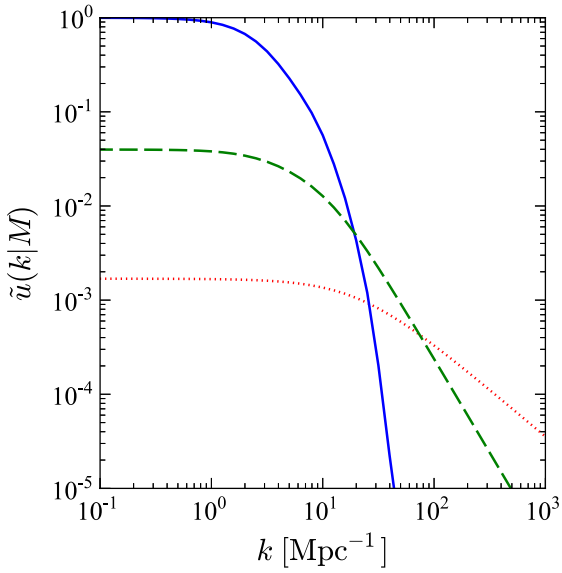

FIG. 18 (color online). Fourier transform of the lines in Fig. 17.

[1] G. Jungman, M. Kamionkowski, and K. Griest, Phys. Rep. **267**, 195 (1996).
[2] L. Bergstrom, Rep. Prog. Phys. **63**, 793 (2000).
[3] G. Bertone, D. Hooper, and J. Silk, Phys. Rep. **405**, 279 (2005).
[4] P. Ullio, L. Bergstrom, J. Edsjo, and C. G. Lacey, Phys. Rev. D **66**, 123502 (2002).
[5] J. E. Taylor and J. Silk, Mon. Not. R. Astron. Soc. **339**, 505 (2003).
[6] S. Ando, Phys. Rev. Lett. **94**, 171303 (2005).
[7] T. Oda, T. Totani, and M. Nagashima, Astrophys. J. **633**, L65 (2005).
[8] L. Pieri, G. Bertone, and E. Branchini, Mon. Not. R. Astron. Soc. **384**, 1627 (2008).
[9] S. Ando and E. Komatsu, Phys. Rev. D **73**, 023521 (2006).
[10] S. Ando, E. Komatsu, T. Narumoto, and T. Totani, Phys. Rev. D **75**, 063519 (2007).
[11] S. Ando, E. Komatsu, T. Narumoto, and T. Totani, Mon. Not. R. Astron. Soc. **376**, 1635 (2007).
[12] F. Miniati, S. M. Koushiappas, and T. Di Matteo, Astrophys. J. **667**, L1 (2007).
[13] A. Cuoco, S. Hannestad, T. Haugbolle, G. Miele, P. D. Serpico, and H. Tu, J. Cosmol. Astropart. Phys. 04 (2007) 013.
[14] A. Cuoco, J. Brandbyge, S. Hannestad, T. Haugboelle, and G. Miele, Phys. Rev. D **77**, 123518 (2008).
[15] J. M. Siegal-Gaskins, J. Cosmol. Astropart. Phys. 10 (2008) 040.
[16] S. K. Lee, S. Ando, and M. Kamionkowski, J. Cosmol. Astropart. Phys. 07 (2009) 007.
[17] M. Taoso, S. Ando, G. Bertone, and S. Profumo, Phys. Rev. D **79**, 043521 (2009).
[18] M. Fornasa, L. Pieri, G. Bertone, and E. Branchini, Phys. Rev. D **80**, 023518 (2009).
[19] J. M. Siegal-Gaskins and V. Pavlidou, Phys. Rev. Lett. **102**, 241301 (2009).
[20] S. Ando, Phys. Rev. D **80**, 023520 (2009).
[21] S. Ando and V. Pavlidou, Mon. Not. R. Astron. Soc. **400**, 2122 (2009).
[22] J. Zavala, V. Springel, and M. Boylan-Kolchin, Mon. Not. R. Astron. Soc. **405**, 593 (2010).
[23] A. Ibarra, D. Tran, and C. Weniger, Phys. Rev. D **81**, 023529 (2010).
[24] J. M. Siegal-Gaskins, R. Reesman, V. Pavlidou, S. Profumo, and T. P. Walker, Mon. Not. R. Astron. Soc. **415**, 1074 (2011).
[25] A. Cuoco, A. Sellerholm, J. Conrad, and S. Hannestad, Mon. Not. R. Astron. Soc. **414**, 2040 (2011).
[26] M. Fornasa *et al.*, arXiv:1207.0502.
[27] M. Ackermann *et al.* (Fermi LAT Collaboration), Phys. Rev. D **85**, 083007 (2012).
[28] A. Cuoco, E. Komatsu, and J. M. Siegal-Gaskins, Phys. Rev. D **86**, 063004 (2012).
[29] L. Gao, C. S. Frenk, A. Jenkins, V. Springel, and S. D. M. White, Mon. Not. R. Astron. Soc. **419**, 1721 (2012).
[30] R. C. Gilmore, R. S. Somerville, J. R. Primack, and A. Dominguez, arXiv:1104.0671.
[31] G. Steigman, B. Dasgupta, and J. F. Beacom, Phys. Rev. D **86**, 023506 (2012).
[32] R. K. Sheth and G. Tormen, Mon. Not. R. Astron. Soc. **308**, 119 (1999).
[33] R. K. Sheth, H. J. Mo, and G. Tormen, Mon. Not. R. Astron. Soc. **323**, 1 (2001).
[34] J. F. Navarro, C. S. Frenk, and S. D. M. White, Astrophys. J. **490**, 493 (1997).
[35] G. L. Bryan and M. L. Norman, Astrophys. J. **495**, 80 (1998).
[36] J. S. Bullock, T. S. Kolatt, Y. Sigad, R. S. Somerville, A. V. Kravtsov, A. A. Klypin, J. R. Primack, and A. Dekel, Mon. Not. R. Astron. Soc. **321**, 559 (2001).
[37] A. R. Duffy, J. Schaye, S. T. Kay, and C. Dalla Vecchia, Mon. Not. R. Astron. Soc. **390**, L64 (2008).
[38] W. Hu and A. V. Kravtsov, Astrophys. J. **584**, 702 (2003).
[39] A. M. Green, S. Hofmann, and D. J. Schwarz, Mon. Not. R. Astron. Soc. **353**, L23 (2004).
[40] A. M. Green, S. Hofmann, and D. J. Schwarz, J. Cosmol. Astropart. Phys. 08 (2005) 003.
[41] J. Diemand, B. Moore, and J. Stadel, Nature (London) **433**, 389 (2005).
[42] J. Diemand, M. Kuhlen, and P. Madau, Astrophys. J. **649**, 1 (2006).
[43] S. Profumo, K. Sigurdson, and M. Kamionkowski, Phys. Rev. Lett. **97**, 031301 (2006).
[44] A. A. Abdo *et al.* (Fermi-LAT Collaboration), Phys. Rev. Lett. **104**, 101101 (2010).
[45] A. A. Abdo *et al.* (Fermi-LAT Collaboration), Astrophys. J. **720**, 435 (2010).
[46] J. Han, C. S. Frenk, V. R. Eke, L. Gao, S. D. M. White, A. Boyarsky, D. Malyshev, and O. Ruchayskiy, Mon. Not. R. Astron. Soc. **427**, 1651 (2012).
[47] B. D. Fields, V. Pavlidou, and T. Prodanovic, Astrophys. J. **722**, L199 (2010).
[48] F. W. Stecker and T. M. Venters, Astrophys. J. **736**, 40 (2011).
[49] R. Makiya, T. Totani, and M. A. R. Kobayashi, Astrophys. J. **728**, 158 (2011).
[50] B. C. Lacki, S. Horiuchi, and J. F. Beacom, arXiv:1206.0772.
[51] T. Narumoto and T. Totani, Astrophys. J. **643**, 81 (2006).
[52] Y. Inoue and T. Totani, Astrophys. J. **702**, 523 (2009); **728**, 73(E) (2011).
[53] K. N. Abazajian, S. Blanchet, and J. P. Harding, Phys. Rev. D **84**, 103007 (2011).
[54] M. Ajello *et al.*, Astrophys. J. **751**, 108 (2012).
[55] V. Springel, J. Wang, M. Vogelsberger, A. Ludlow, A. Jenkins, A. Helmi, J. F. Navarro, C. S. Frenk, and S. D. M. White, Mon. Not. R. Astron. Soc. **391**, 1685 (2008).
[56] M. Ackermann *et al.* (Fermi-LAT Collaboration), Phys. Rev. Lett. **107**, 241302 (2011).
[57] A. Geringer-Sameth and S. M. Koushiappas, Phys. Rev. Lett. **107**, 241303 (2011).
[58] S. Ando and D. Nagai, J. Cosmol. Astropart. Phys. 07 (2012) 017.